



Impaired capillary-to-arteriolar electrical signaling after traumatic brain injury

Amreen Mughal¹, Adrian M Sackheim², Maria Sancho¹, Thomas A Longden³, Sheila Russell², Warren Lockette⁴, Mark T Nelson^{1,5} and Kalev Freeman^{1,2}

Abstract

Traumatic brain injury (TBI) acutely impairs dynamic regulation of local cerebral blood flow, but long-term (>72 h) effects on functional hyperemia are unknown. Functional hyperemia depends on capillary endothelial cell inward rectifier potassium channels (Kir2.1) responding to potassium (K⁺) released during neuronal activity to produce a regenerative, hyperpolarizing electrical signal that propagates from capillaries to dilate upstream penetrating arterioles. We hypothesized that TBI causes widespread disruption of electrical signaling from capillaries-to-arterioles through impairment of Kir2.1 channel function. We randomized mice to TBI or control groups and allowed them to recover for 4 to 7 days post-injury. We measured in vivo cerebral hemodynamics and arteriolar responses to local stimulation of capillaries with 10 mM K⁺ using multiphoton laser scanning microscopy through a cranial window under urethane and α -chloralose anesthesia. Capillary angio-architecture was not significantly affected following injury. However, K⁺-induced hyperemia was significantly impaired. Electrophysiology recordings in freshly isolated capillary endothelial cells revealed diminished Ba²⁺-sensitive Kir2.1 currents, consistent with a reduction in channel function. In pressurized cerebral arteries isolated from TBI mice, K⁺ failed to elicit the vasodilation seen in controls. We conclude that disruption of endothelial Kir2.1 channel function impairs capillary-to-arteriole electrical signaling, contributing to altered cerebral hemodynamics after TBI.

Keywords

Cerebral blood flow, capillary endothelial cells, functional hyperemia, inward rectifier K⁺ channels (Kir2.1), traumatic brain injury

Received 20 May 2020; Revised 28 July 2020; Accepted 31 August 2020

Introduction

Between 64 to 74 million individuals worldwide¹ are believed to sustain a traumatic brain injury (TBI) each year, resulting in more than 2.5 million TBI-related emergency department visits and 56,000 deaths in the United States alone.^{2,3} The elevated risks of blast injury in active duty military personnel and chronic traumatic encephalopathy in football players and other athletes,⁴ provide further rationale for studying the mechanisms that contribute to long-term disabilities after TBI.^{5,6}

Neurons in the brain have a limited energy reserve and rely on a precise, moment-to-moment strategy to supply vast metabolic demands. Our previous work has demonstrated that capillary endothelial cells (cEC) are the essential sensors of neuronal metabolic needs and

¹Department of Pharmacology, University of Vermont, Burlington, VT, USA

²Department of Surgery, University of Vermont, Burlington, VT, USA

³Department of Physiology, School of Medicine, University of Maryland, Baltimore, MD, USA

⁴Department of Internal Medicine, Wayne State University School of Medicine, Detroit, MI, USA

⁵Division of Cardiovascular Sciences, University of Manchester, Manchester, UK

Corresponding author:

Kalev Freeman, Department of Surgery, University of Vermont, Given E301, 89 Beaumont Avenue, Burlington, VT 05405-0068, USA.

Email: kalev.freeman@uvm.edu

regulate cerebral blood flow (CBF) by communicating with upstream penetrating arterioles.⁷ This communication depends on electrical signaling initiated by cECs Kir2.1 channels that rapidly respond to the elevated extracellular K^+ released during neuronal activity. The hyperpolarization resulting from Kir2.1 channel opening propagates along the vascular wall in a retrograde direction to dilate upstream penetrating arterioles and increase blood flow.

The delicate network of interconnected vessels and capillaries comprising the cerebral vasculature is at risk of disruption by both the mechanical force of a brain injury and through subsequent hemorrhagic expansion, edema, and inflammation.^{8–11} Secondary problems with vascular function, including significant decreases in global and regional CBF, contribute to adverse outcomes such as cognitive decline, ischemic stroke, depression, and dementia.^{12–15} Abnormal vascular reactivity may persist for months even in the absence of visible structural injury to the tissue parenchyma.⁴ While significant reductions in global and regional CBF after severe brain trauma have been recognized for over 40 years,^{4,11,16–18} little is known about the long-term effects of more mild, survivable TBI on cerebral capillary function and the dynamic regulation of local CBF responses during neurovascular coupling. This critical knowledge gap limits progress in understanding and treating long-term disabilities after TBI.

To address this problem, we tested the hypothesis that TBI causes widespread disruption of electrical signaling from capillary-to-arterioles through impairment of cEC Kir2.1 channel function. We examined regulation of CBF in an apparently unaffected cortical capillary bed 4 to 7 days after fluid percussion brain injury. We found that even in apparently normal appearing brain regions remote from the primary injury, K^+ -induced hyperemia at the level of the capillary microcirculation is significantly impaired relative to controls. Next, we provide evidence of reduced Kir2.1 channel function in isolated cECs. Finally, pressurized cerebral arteries from TBI mice exhibited decreased K^+ -induced vasodilation despite having normal spontaneous myogenic tone. Together, these results provide a novel mechanism linking endothelial Kir2.1 channelopathy to impaired functional hyperemia 4 to 7 days after TBI.

Methods

Animal husbandry

Male C57BL/6J mice (Jackson Laboratories, Bar Harbor, ME), aged 8–12 weeks, were selected at random to either TBI surgery or control treatment groups. Blinding of investigators to group allocation was not feasible because the TBI group had a visible

surgical scar. Naïve mice, not exposed to any surgical procedures, were used as controls for most experiments. For the *in vivo* studies, we also studied sham controls, consisting of mice subjected to the surgical procedure but without fluid percussion injury. Animals in the experimental TBI group were anesthetized, administered a fluid percussion injury, and allowed to recover for three post-operative days prior to experimentation. Mice were kept on a 12 h light/dark cycle, with *ad libitum* access to food and water and were housed in groups of five. All studies were conducted in accordance with the Guidelines for the Care and Use of Laboratory Animals (National Institute of Health), Guidelines for Survival Rodent Surgery (National Institute of Health) and approved by the Institutional Animal Care and Use Committee of the University of Vermont. All procedures were conducted and reported in accordance with the ARRIVE guidelines (Animal Research: Reporting *In Vivo* Experiments) (<https://www.nc3rs.org.uk/arrive-guidelines>).

Experimental traumatic brain injury

A fluid percussion injury method was used to induce a TBI. Mice were anesthetized with 2%–5% isoflurane, and the animal's head was stereotaxically restrained. A craniotomy was performed midway between lambda and bregma, 2 mm lateral to the sagittal suture, by drilling a 3 mm diameter hole through the skull into the underlying extradural space using a variable speed power drill. A custom stainless steel, hollow intracranial screw with a 2 mm internal diameter was fitted into the craniotomy hole. The intracranial screw was filled with 0.9% normal saline and attached with tubing to the fluid percussion apparatus. A weighted pendulum was released to impact the fluid percussion device and induce TBI. During injury, the intracranial pressure and its peak pressure by the fluid percussion wave were recorded using an inline pressure transducer connected to a data acquisition system and measured in pounds per square inch (PSI) (Instrumentation and Modeling Facility, University of Vermont, VT). We previously determined a level of injury at 37 PSI which was survivable in the majority of animals (66% survival) but with demonstrable neurologic outcomes.¹⁹ All animals received 0.02 mg/kg subcutaneous buprenorphine for analgesia while under anesthesia and to treat postoperative pain. Animals were studied using *in vivo* imaging, or euthanized, approximately 1 week after injury (4–7 days).

In vivo imaging of cerebral hemodynamics

Craniotomy and *in vivo* imaging were performed as previously described.⁷ Briefly, mice were anesthetized

with isoflurane (5% induction and 2% maintenance). The skull was exposed, a stainless-steel head plate was attached, and a small circular cranial window was created above somatosensory cortex contra-lateral to the side of injury. Approximately, 150 μ L of a 3-mg/mL solution of FITC-dextran (MW 150 kDa) in sterile saline was injected intravenously into the retro-orbital sinus²⁰ to allow visualization of the cerebral vasculature and contrast imaging of red blood cells (RBCs). Upon conclusion of surgery, isoflurane anesthesia was replaced with α -chloralose (50 mg/kg) and urethane (750 mg/kg). Body temperature was maintained at 37°C throughout the experiment using an electric heating pad. The brain was continuously perfused with artificial cerebrospinal fluid (aCSF) containing (in mM) 124 NaCl, 3 KCl, 2 CaCl₂, 2 MgCl₂, 1.25 NaH₂PO₄, 26 NaHCO₃, and 4 glucose. A pipette was introduced into the cortex, maneuvered adjacent to the capillary under study and pressurized injections (200–300 ms, 5 ± 1 PSI) of 10 mM K⁺ with tetramethylrhodamine isothiocyanate (TRITC, MW 150 kDa; 0.06 mg/mL)-labeled dextran were ejected directly onto the capillary. RBC flux and velocity data were collected by line scanning the capillary of interest at 5 kHz. Structural analyses were performed by collecting 3D-stacks on a field of the x–y dimensions (424 \times 424 μ m) plus \sim 300 μ m in the z axis. Images were acquired through a Zeiss 20 \times Plan Apochromat 1.0 NA DIC VIS-IR water-immersion objective mounted on a Zeiss LSM-7 multiphoton microscope (Zeiss, USA) coupled to a Coherent Chameleon Vision II Titanium-Sapphire pulsed infrared laser (Coherent, USA). FITC and TRITC were excited at 820 nm, and emitted fluorescence was separated through 500–550-nm and 570–610-nm band-pass filters, respectively.

Cortical capillary structure analysis

Composite TIFF files of 3D-stacks generated from control and TBI mice were analyzed using an automated image analysis program (Autotube; freely available at <https://github.com/autotubularity/autotube>).²¹ Briefly, images (8-bit TIFF files) along with imaging parameters were included in the software. Noise correction and tube detection were performed using BM3D and MultiOtsu filters, respectively. Pial and penetrating vessels were manually removed before the analysis. Output data including number of branching points, vessel width and average vessel length, automatically calculated by the program were then exported as Excel files and used for reporting results.

Electrophysiology

Capillary ECs were obtained from mouse brain as previously reported.⁷ In brief, a small piece of cortex (\sim 200–250 μ m-thick) was placed in ice-cold aCSF and mechanically disrupted using a Dounce homogenizer. Debris was discarded by passing the homogenate through a 62 μ m nylon mesh. Retained capillary fragments were enzymatically digested by incubating in an isolation solution composed of (in mM) 55 NaCl, 80 Na-glutamate, 5.6 KCl, 2 MgCl₂, 4 glucose and 10 HEPES (pH 7.3), containing 0.5 mg/ml neutral protease, 0.5 mg/ml elastase (Worthington, USA) and 100 μ M Ca²⁺, for 23 min at 37°C. Thereafter, the sample was incubated with 0.5 mg/ml collagenase type I (Worthington, USA) for an extra 2 min. The cell suspension was filtered, and the remaining tissue was washed to remove the enzymes and triturated with a fire-polished glass Pasteur pipette. Single cells and small capillary segments were stored in ice-cold isolation medium for use the same day within \sim 5 h.

Conventional patch-clamp electrophysiology was used to measure whole-cell currents in isolated cECs. Briefly, currents were amplified using an Axopatch 200 amplifier, filtered at 1 kHz, digitized at 10 kHz, and stored on a computer for offline analysis with Clampfit 10.7 software (Molecular Devices, USA). Patch pipettes were pulled from borosilicate, microcapillary tubes (1.5-mm OD, 1.17-mm ID; Sutter Instruments, USA), fire-polished (resistance of 3–6 M Ω) and backfilled with a solution containing (in mM) 10 NaOH, 11.4 KOH, 128.6 KCl, 1.1 MgCl₂, 2.2 CaCl₂, 5 EGTA, and 10 HEPES (pH 7.2). The bath solution consisted of (in mM) 80 NaCl, 60 KCl, 1 MgCl₂, 10 HEPES, 4 glucose, and 2 CaCl₂ (pH 7.4). The mean capacitance of capillary ECs averaged 9.89 ± 0.43 pF. All experiments were performed at room temperature (\sim 22°C).

Ex vivo arterial diameter measurements

Mice were euthanized, and a full craniectomy was performed to expose the brain which was then dissected and placed into cold (4°C) HEPES-buffered physiological saline solution (HEPES-PSS) with the following composition (in mM): 134 NaCl, 6 KCl, 2 CaCl₂, 1 MgCl₂, and 7 glucose (pH 7.4). The brain was then pinned out in a silicone-lined dissecting dish and the posterior cerebral artery (PCA), contralateral to the fluid percussion injury, was dissected free from the surrounding dura and pia mater. PCAs were then cannulated in a pressure myograph chamber (Living Systems Instrumentation, USA) using nylon sutures. Residual blood and debris were flushed out of the lumen prior to cannulating the distal end of the artery. The pressure

myograph was placed on the stage of an inverted microscope (AE31; Motif, Canada) and continuously superfused with oxygenated (20% O₂; 5% CO₂; 75% N₂) aCSF maintained at 37°C. Intraluminal pressure was controlled using a pressure servo system (Living Systems Instrumentation, USA), and blood vessel diameters were measured using edge-detection software (IonOptix, USA).

To assess myogenic response of individual vessels, arteries were allowed to equilibrate at 10 mm Hg for ~10 min. The intraluminal pressure increased to 80 mm Hg, and vessels were allowed to develop spontaneous myogenic tone. Vessels with pressure leaks or those without intact endothelium, tested using 1 μM NS309 (Cayman Chemical, USA), were not studied. To assess vasodilatory function in response to elevated K⁺, arteries were pressurized to 80 mm Hg, allowed to develop spontaneous myogenic tone, and equilibrated for 30 min for measurement of intraluminal diameter (baseline). The bath solution was then changed to an elevated potassium aCSF (10 mM K⁺) to elicit vasodilation. The arteries were then washed with physiological aCSF, allowed to recover, and the bath was then exchanged with 0 Ca²⁺ aCSF with 100 μM diltiazem to elicit maximal passive diameter. Percentage of myogenic tone at 80 mm Hg was calculated as the percentage decrease of the vessel diameter using the following equation: tone (%) = [(passive diameter – active diameter)/passive diameter] × 100. The percentage of K⁺-induced vasodilation was measured at the point of peak dilation and calculated as: vasodilation (%) = [(diameter after K⁺ administration – baseline diameter)/baseline diameter].

Data analysis and statistics

Patch-clamp data were analyzed using Clampfit 10.7 software. Changes in arteriolar diameter were calculated from the average luminal diameter measured over the last 10 s of stimulation. The shape of arterioles during in vivo imaging depends on the focal plane and can appear as a circle or oval. We measured diameter of both short and long axes, at baseline and after stimulation, and reported the change in diameter as an average. This allowed us to normalize each blood vessel to its own baseline, eliminating the impact of arteriole shape on the measurements. RBC flux and velocity were analyzed offline using custom software (SparkAn, Adrian Bonev, University of Vermont, USA). Flux data were binned at 1-s intervals. Mean baseline velocity and flux data for summary figures were obtained by averaging the baseline (~6 s) for each measurement before pressure ejection of 10 mM K⁺. The peak response was defined as the peak 1-s flux bin after delivery of K⁺ within the remaining scanning

period (~36 s). Because flux and velocity are correlated, the average velocity of all cells in the peak flux bin was reported for velocity summary data. The depth of capillaries below the surface was estimated from z-stack series acquired before pipette placement. Results are expressed as mean ± standard deviation (SD), and *n* refers to the number of animals used, unless otherwise stated. All data sets were tested for normal distribution using the Shapiro–Wilk test, and a subsequent unpaired *t* test or Mann–Whitney test was applied based on parametric or non-parametric distribution, respectively. A paired *t* test or Wilcoxon test was applied based on parametric or non-parametric distribution, respectively, for paired data. Values were considered significantly different when *p* < 0.05. For in vivo experiments, we compared naïve control group with TBI. The same naïve control group was compared again with sham controls to rule out any potential effect of the surgical procedures. For electrophysiology experiments, power analyses confirmed that a sample size of *n* = 6 per group was enough to observe statistical significance. Sample sizes for all other experimental preparations were estimated using our previous experience.

Results

Cortical capillary vascular structure is preserved after TBI

We used a craniotomy-based approach on the right side of the somatosensory cortex to analyze vascular structures visualized with FITC-dextran 4 to 7 days after injury to the contralateral hemisphere. We mapped cortical vasculature down to ~layer III with average Z depth of 300 ± 10 μm (0.5 μm z-steps) from the pial vessel border. We classified vessels as penetrating arterioles, venules, or capillaries according to their orientation and branch orders. Interestingly, fluid percussion injury on the left cortex caused no structural damage to the contralateral cortical vasculature. Our automated 3D structural analyses show that the density of capillary webs surrounding penetrating arterioles did not change post-injury. Moreover, average capillary diameter, length, and branch point analyses indicate an absence of macroscopic changes in cortical capillary vasculature post-injury (Figure 1).

K⁺-induced hyperemia is impaired after TBI

We used in vivo multiphoton imaging for contrast imaging of blood flow to test our hypothesis that K⁺-induced hyperemia is impaired in TBI. After performing z-stacks, we identified a field of view and applied K⁺ to capillary beds and measured dynamic local CBF

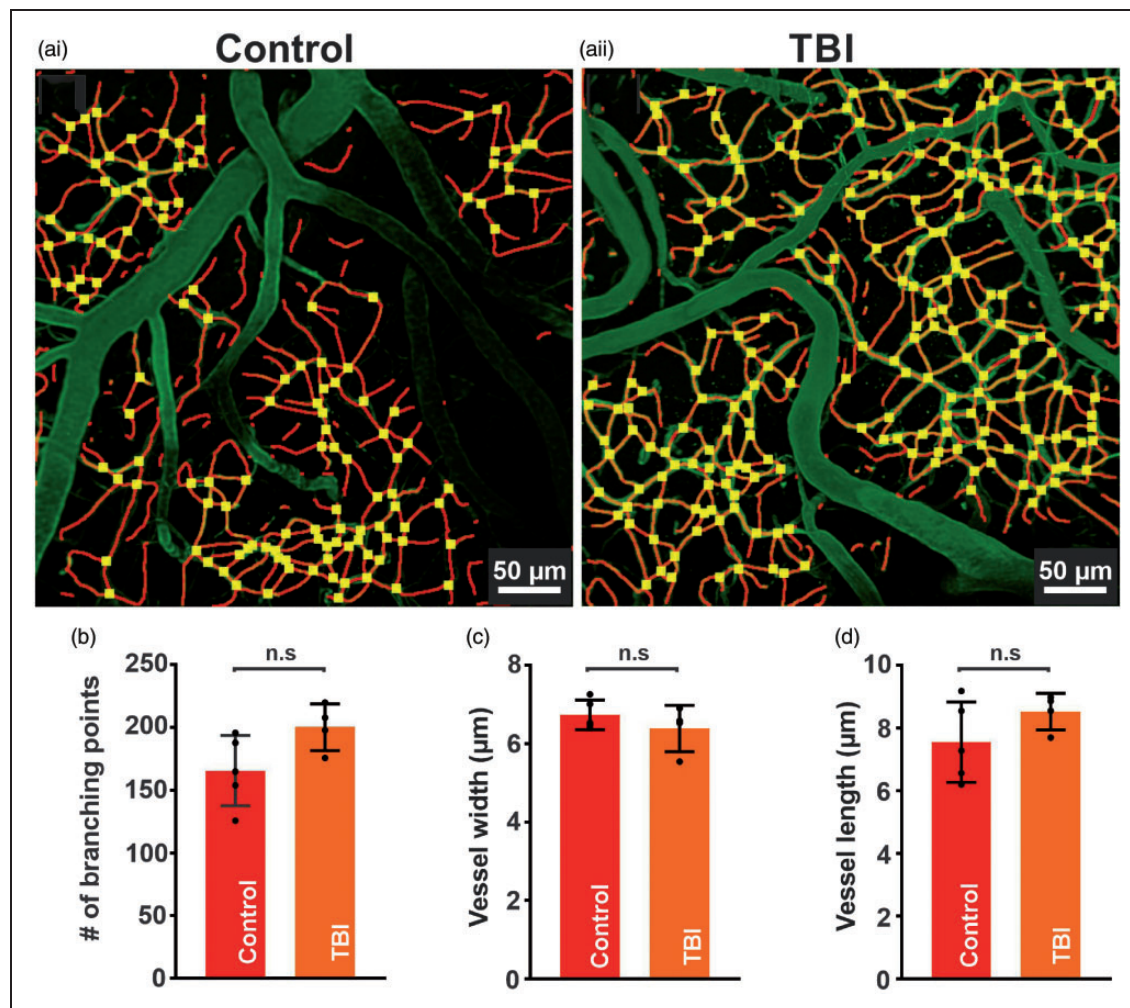


Figure 1. Cortical capillary structure is preserved after TBI. (a) In vivo 3D-images processed by autotube showing cortical capillaries from a control (i) and TBI (ii) mouse. Block width = $425 \times 425 \mu\text{m}$, block depth = $300 \mu\text{m}$. Summary data comparing various control and TBI structural analyses. No significant differences were present in (b) the number of branch points (166 ± 28 , $n = 5$ vs 201 ± 19 , $n = 4$ branch points, n.s., unpaired t test) (c) vessel width (7 ± 0.4 , $n = 5$ vs $6 \pm 1 \mu\text{m}$, $n = 4$, n.s., unpaired t test), or (d) vessel length (8 ± 1 , $n = 5$ vs $9 \pm 1 \mu\text{m}$, $n = 4$, n.s., unpaired t test) between control and TBI mice, respectively. Data are expressed as mean \pm SD.

responses. We quantified changes in capillary RBC flux, velocity, and upstream arteriolar diameter in response to local pressure injections of 10mM K^+ administered through a micropipette around post arteriolar capillaries (third or fourth order branch from arterioles). We previously established that placement of the pipette in the brain under these conditions restricts agent delivery to the capillary bed under study and produces minimal displacement of the surrounding tissue.⁷ In control mice, the administration of K^+ caused a rapid and robust increase in both RBC flux ($110 \pm 63\%$, $n = 8$, $*p = 0.004$, paired t test) and velocity ($95 \pm 46\%$, $n = 8$, $*p = 0.002$, paired t test). Conversely, exposure of capillaries in TBI mice to 10mM K^+ did not produce a significant increase of RBC flux ($23 \pm 17\%$, $n = 8$, n.s., paired t test) or

velocity ($29 \pm 62\%$, $n = 8$, n.s., paired t test) from the baseline condition (Figure 2).

Because it is the dilation of upstream arterioles that ultimately promotes a hyperemic response in the capillary bed where the triggering K^+ signal originates, we further examined capillary-to-arteriole communication by measuring the change in diameter of these arterioles in vivo. We found that local pressure injection of K^+ (10mM) onto a capillary bed caused robust vasodilation of the connected upstream arteriole ($23 \pm 4\%$, $n = 7$, $*p < 0.0001$, paired t test) in controls, but this manipulation did not increase arteriolar diameter in TBI mice (Figure 3). To address the potential caveat that the anesthesia and surgical procedures might impact Kir function in vivo, we performed a subset of experiments in mice subjected to an identical surgical

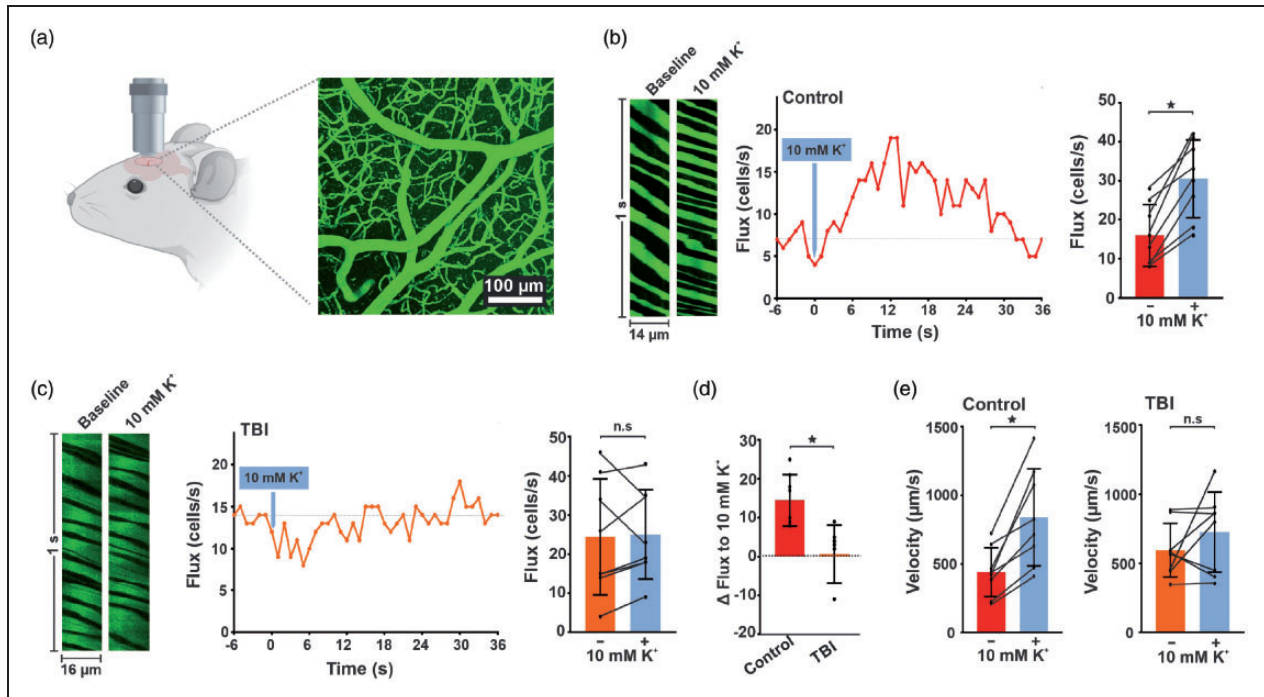


Figure 2. K⁺-induced hyperemia is impaired in vivo in TBI mice. (a) In vivo imaging approach. A cranial window was prepared over the somatosensory cortex and imaged using 2-photon laser-scanning microscopy. (b and c) Left: baseline and peak distance–time plots of capillary line scans showing hyperemia to the ejection of 10 mM K⁺ onto a capillary. RBCs passing through the line-scanned capillary appear as black shadows against green fluorescent plasma. Middle: typical experimental time-course of RBC flux binned at 1-s intervals before and after pressure ejection of 10 mM K⁺ (300 ms, 5 ± 1 psi; gray arrow) onto a capillary, demonstrating hyperemia to K⁺ delivery. Right: summary RBC flux responses to 10 mM K⁺ in (b) control and (c) TBI mice. K⁺ delivery caused significant hyperemia in control (16 ± 8 vs 31 ± 10 cells/s, n = 8 paired experiments, 6 mice; *p = 0.0004, paired t test), but not in TBI (24 ± 15 vs 25 ± 11 cells/s, n = 8 paired experiments, 6 mice; p = 0.819, paired t test) mice when compared to their baseline prior to K⁺ application, respectively. (d) The percent change in RBC flux after 10 mM K⁺ application is significantly decreased in TBI mice when compared to controls (0.6 ± 7 vs 15 ± 7%, n = 8; *p = 0.0008, Mann-Whitney test). (e) K⁺-induced hyperemia caused a significant increase in flux velocity in control (left) (441 ± 179 vs 840 ± 353 μm/s, n = 8 paired experiments, 6 mice; *p = 0.0022, paired t test) but not in (right) TBI (594 ± 195 vs 726 ± 289 μm/s, n = 8 paired experiments, 6 mice; n.s., paired t test) mice when compared to their respective baseline controls. Data are expressed as mean ± SD.

procedure without fluid percussion injury. We found that K⁺-induced hyperemia is comparable in naïve and sham control mice (Supplementary Figure 1). These findings support our premise that the TBI, and not the surgical procedure, explains the observed disruption in functional hyperemia.

cEC Kir2.1 channel current density is reduced in TBI mice

Patch-clamp electrophysiology was next used to explore whether cEC Kir2.1 channel function and their involvement in K⁺-induced hyperemia is compromised after TBI. Whole-cell currents were measured in cECs isolated from TBI mice 4 to 7 days post-injury and compared to the control subset of mice. We quantified whole-cell currents in response to a voltage ramp (400 ms, from −140 to +40 mV) in cells bathed in

60 mM [K⁺]_o, used to amplify the inward component of Kir2.1 channel currents. Under these conditions, the K⁺ equilibrium potential (E_K) was −23 mV. As shown in Figure 4(a)–(b), inward currents, observed at negative potentials to E_K, were significantly smaller in cECs isolated from TBI mice, consistent with an impairment of Kir channel function. BaCl₂ (100 μM), a selective Kir2 channel blocker, was employed to isolate the Kir2.1 component from the total current density. Ba²⁺-sensitive currents were significantly reduced by 64% in TBI cECs (−4 ± 1 pA/pF, n = 11 cells) compared with controls (−11 ± 2 pA/pF, n = 8 cells; Figure 4(c)). These findings collectively suggest that impaired K⁺-induced hyperemia is associated with reduced cEC Kir2.1 channel activity. Because Kir channels are critical not only for capillary-to-arteriolar signaling but also for K⁺-induced vasodilation of cerebral arteries, we proceeded to examine K⁺

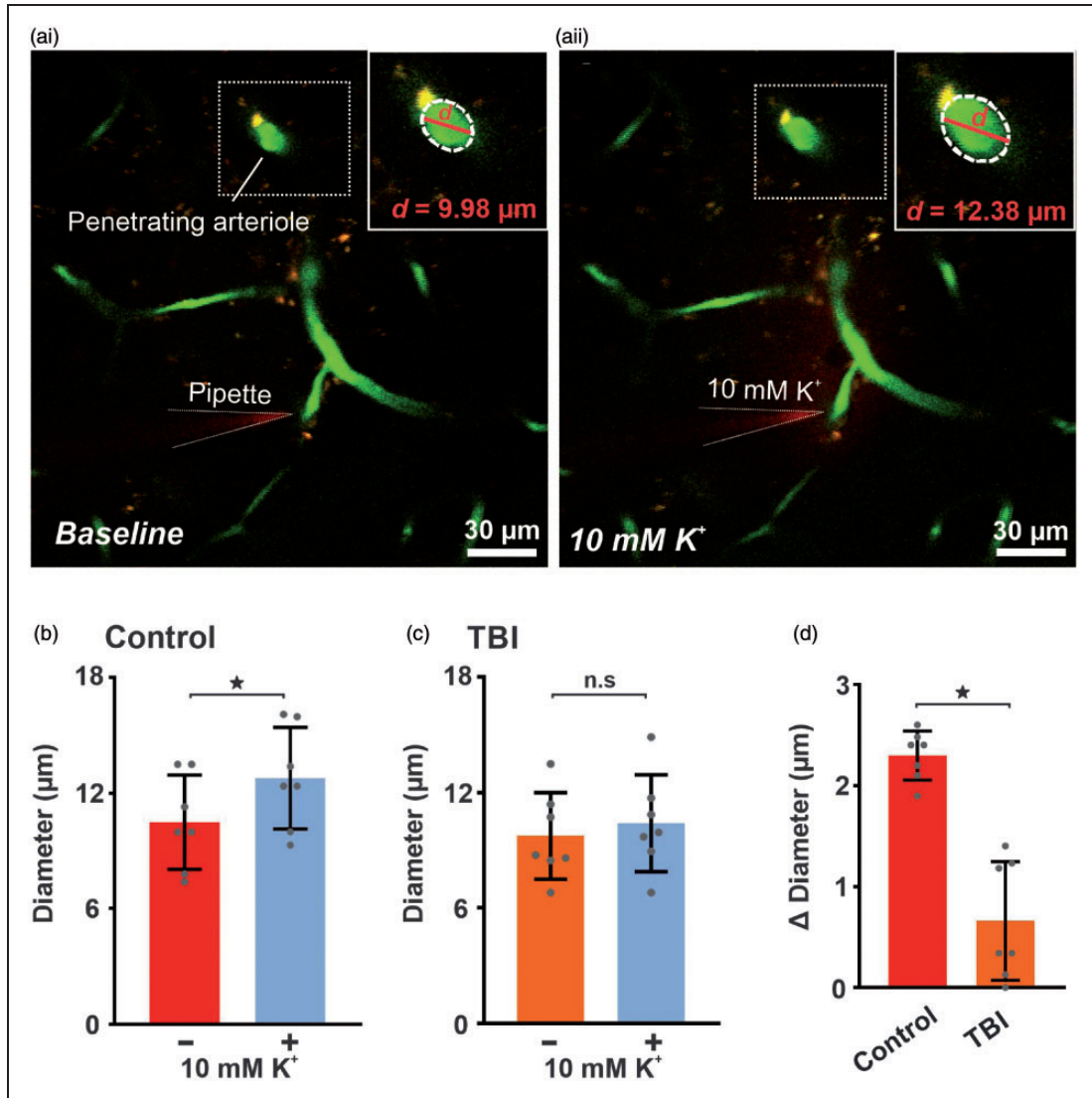


Figure 3. K^+ -induced capillary-to-arteriolar signaling is impaired in vivo after TBI. Micrograph illustrating pipette placement adjacent to a third-order capillary for in vivo monitoring of the diameter of the upstream feed arteriole (boxed) in ('ai') control and ('aii') TBI mice. Note the dilation in the penetrating arteriole (boxed). Magnification of the boxed areas around the penetrating arteriole, illustrate the magnitude of dilation evoked by capillary stimulation with 10 mM K^+ . Summary data showing arteriole diameter before and after capillary application of 10 mM K^+ , which produced significant upstream arteriole dilation when comparing diameters pre- and post-application of 10 mM K^+ in (b) control (10 ± 2 vs $13 \pm 3 \mu\text{m}$, $n = 7$ paired experiments, 6 mice; $*p < 0.0001$, paired t test) but not in (c) TBI (10 ± 2 vs $10 \pm 3 \mu\text{m}$, $n = 7$ paired experiments, 6 mice; n.s., paired t test) mice. (d) The change in diameter after application of 10 mM K^+ is significantly impaired in TBI ($0.7 \pm 0.6 \mu\text{m}$, $n = 7$, $*p < 0.001$, unpaired t test) mice when compared to controls ($2 \pm 0.2 \mu\text{m}$, $n = 7$). Data are expressed as mean \pm SD.

responses in isolated, pressurized pial vessels to demonstrate functional consequences of altered Kir conductance.

Vasodilatory responses of pial arteries to K^+ are diminished following TBI

Potassium has long been known to have profound vasoactive effects on blood vessels, producing vasodilation in small doses and vasoconstriction in large

doses, and the importance of local K^+ release in dynamic regulation of local CBF during neurovascular coupling has been well established.²² In the cerebral circulation, increases in the extracellular K^+ concentration within the range of 1 to 15 mM normally causes rapid and potent dilation of small arteries.^{23–25} Isolated pial arteries (PCAs) harvested from TBI ($23 \pm 16\%$ tone, $n = 7$) and control ($15 \pm 4\%$ tone, $n = 7$) mice both developed spontaneous myogenic tone when pressurized to 80 mm Hg (n.s., unpaired t test). As

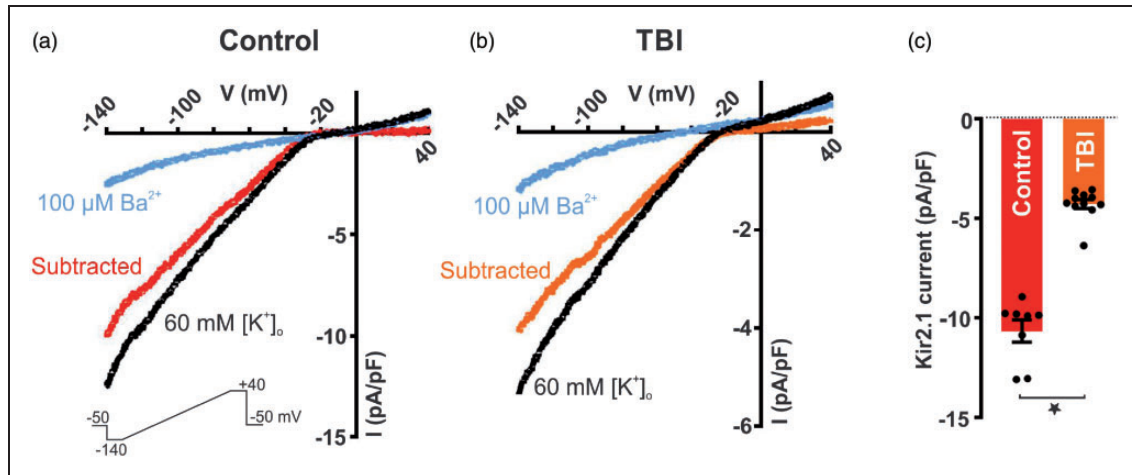


Figure 4. Kir_{2.1} channel current density is markedly reduced in ECs isolated from TBI mice. Inwardly rectifying current (black) was evoked by a 400-ms voltage ramp (−140 to +40 mV; lower inset) in capillary endothelial cells isolated from control (a) and TBI (b) mice and blocked by 100 μM Ba²⁺. (c) Summary data of Ba²⁺-sensitive current density at peak inward currents (−140 mV) in control (−11 ± 2 pA/pF, n = 8 cells, from 3 mice) and TBI mice (−4 ± 1 pA/pF, n = 11 cells, from 4 mice) (*p < 0.0001, Mann-Whitney test). Data are expressed as mean ± SD.

expected, raising extracellular K⁺ from 3 to 10 mM caused robust dilation in controls (56 ± 32% change in diameter; n = 7), but this response was significantly impaired in TBI mice (26 ± 16% change in diameter; n = 7; *p < 0.05, unpaired *t* test) (Figure 5). This reduced K⁺-induced vasodilation suggests that impaired function of Kir channels following TBI is pervasive and not limited to capillaries.

Discussion

TBI abruptly decreases cerebral perfusion and disrupts hyperemic responses; however, the mechanisms underpinning this disruption are not completely understood. Little is known about the long-term effects of TBI on functional hyperemia at the level of the cortical microcirculation and cECs, particularly in tissue that appears normal after injury tissue, and even less is known about effects at time points greater than 72 h. In the present study, we aimed to understand underlying mechanisms that are associated with impaired K⁺-induced hyperemia 4 to 7 days after TBI.

The capillary EC Kir2.1 channels are a central molecular player in the mechanism of functional hyperemia in the brain, but their role in models of brain injury or ischemia has not been previously studied. Here, we present three important findings: (1) K⁺-induced hyperemia at the level of the capillary microcirculation is impaired 4–7 days after injury, even in normal appearing brain regions remote from the primary TBI injury; (2) cEC Kir2.1 channel function is reduced by 64%, providing a mechanism to explain the impairment in K⁺-induced hyperemia; and (3)

abnormal vascular responses to K⁺ extend to large, pial arteries as well, further reducing CBF. Together, these results indicate that vascular Kir2.1 channelopathy after brain injury contributes to the uncoupling of the neurovascular unit and impairs a critical electrical signal pathway directing local blood supply to active capillary beds.

Cortical capillary structure remote from peri-injury region is preserved after TBI

Magnetic resonance imaging assessment of human subjects with chronic TBI has shown that even normal appearing tissue suffers from significantly diminished vascular reactivity.²⁶ We sought to study cerebral hemodynamics remote from the primary site of injury, so that pathological features such as edema, hemorrhage, and thrombosis would not complicate measurement of local blood flow. Therefore, we imaged the cortical hemisphere contralateral to TBI, remote from the peri-injury region. The qualitative appearance of the vascular bed in the injured brains was indistinguishable from controls. We also applied an automated 3D structural analysis to quantify capillary branching points and density, showing that the microvascular architecture of the TBI brains was not different from controls.

Our results differ from those in a prior study in which rats imaged 1-day post-TBI demonstrated a marked reduction in cerebral microvascular density.²⁷ In a follow-up study, the same group reported that the vascular density near the injured site returned to baseline levels by day 14, but effects on the contralateral site

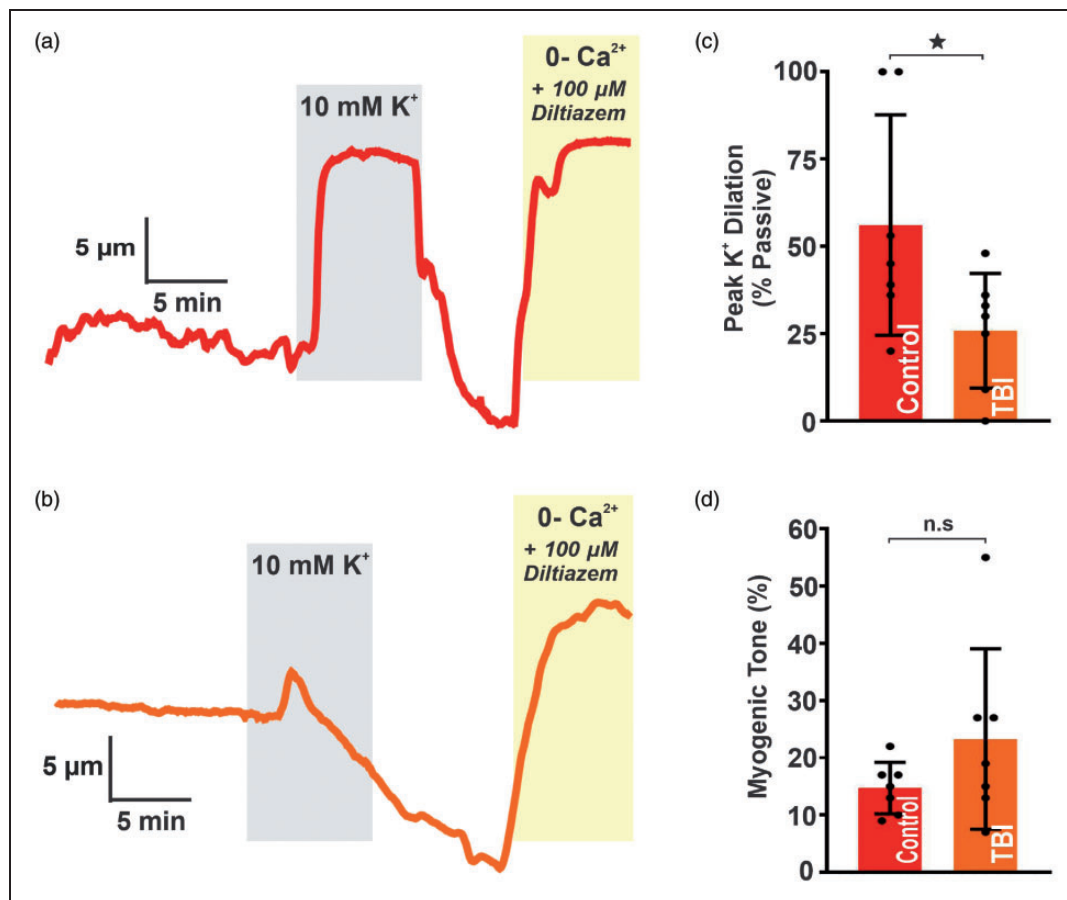


Figure 5. Vascular reactivity is impaired in pial arteries following TBI. Representative traces of lumen diameter in PCAs from (a) control and (b) TBI mice. Extracellular K⁺ was raised from 3 to 10 mM (highlighted in gray). The vasodilatory response was measured at the point of maximal dilation and normalized to maximal diameter (“passive diameter”), obtained in zero Ca²⁺ aCSF with 100 μM diltiazem at the end of each experiment. (c) Summary data for peak diameter elicited by 10 mM K⁺ in PCAs from control (56 ± 32%; n = 7) and TBI (26 ± 16%; n = 7) mice (*p < 0.05; unpaired t test). (d) Summary data for spontaneous myogenic tone at 80 mm Hg in PCAs from control (15 ± 4%; n = 7) and TBI (23 ± 16%; n = 7) mice (n.s.; unpaired t test). Data are expressed as mean ± SD.

were not included.¹¹ While we were unable to identify any differences in vessel structure or density 4 to 7 days after injury, it is possible that there was an earlier loss of vascular features that may have recovered by day 7. Additionally, we cannot exclude the possibility that anatomic pathology in the vascular beds we studied would have been revealed through other approaches. For example, despite an overall normal angio-architectonic distribution, microvascular casts of cortical brain vessels from humans who died after severe TBI demonstrated disarrangement of endothelial cells, resulting in enlargement of the perivascular space with collapsed lumens.²⁸ Others have also shown a diffuse microvascular thrombosis throughout the cortical vessels of patients who died within 48 h of injury.²⁹ A study of teenage athletes who died after mild closed-head injury provided evidence of microvascular injury and perivascular neuroinflammation.³⁰ In either case, we did not observe any qualitative or

quantitative effects of TBI on vascular morphology in the contralateral cortical hemisphere. Future studies with multiple time points and longer duration are warranted to decipher the progression and recovery cycle associated with structural changes.

Disruption of capillary-to-arteriolar communication and impaired hyperemic response

Although there is extensive literature reporting acutely altered global and regional CBF after brain injury, little is known about the regulation of blood flow at the capillary level after TBI. Ion channels play a critical role in the control of CBF and the uncoupling of capillary-to-arteriolar signaling in the cerebral vasculature renders the brain at risk of ischemia, metabolic deficiencies, and vascular spasm.³¹ Previously, we demonstrated that brain cECs constitute a neuronal activity-sensing network that is capable of initiating

long-range electrical (hyperpolarizing) signals in response to neuronal activity that rapidly propagate upstream to cause dilation of upstream feeding arterioles to increase blood flow locally at the site of signal initiation.⁷ To our knowledge, the underlying mechanisms associated with impaired functional hyperemia including capillary-to-arteriolar communication have not been previously studied after TBI.

Here, we provide novel evidence that – even in the absence of structural changes to cortical tissue – dynamic increases in local RBC flux and velocity triggered by capillary exposure to K^+ were absent following injury. Furthermore, we show that TBI resulted in a significant impairment in arteriolar dilation in response to capillary stimulation. Together, these results demonstrate that the active regulation of local CBF through capillary-to-arteriolar electrical signaling is disrupted after TBI. These results are important, because the microvascular control system is crucial to local CBF allocation in response to changing metabolic needs.³² Occlusion of even one penetrating arteriole has been shown to result in infarction and cognitive deficit.³³ Although little is known about the regulation of blood flow at the capillary level after TBI, a biophysical model of oxygen transport in tissue after TBI demonstrated reduced capillary transit time resulted in reduced oxygenation, contributing to profound changes in CBF.⁹ Moreover, the combination of increased intracranial pressure, cerebral vasospasm, and mechanical injury to intracranial vessels results in unstable oxygen tension after TBI.³⁴ In animal models, transient dips in tissue oxygen tension drive capillary hyperemia through direct effects on erythrocyte deformability and flow velocity.³⁵ Thus, unstable oxygen tension after TBI may also impact the impaired hyperemic response, independent of Kir channel function.

Our results are novel in the context of prior human and animal studies that report changes in global and regional CBF after brain injury. Human studies have shown both global and regional impairments in CBF after TBI correlate with adverse clinical outcomes.^{16–18,26,36–39} The majority of studies were focused on the acute response to TBI, but in one recent study, individuals were studied at multiple time points (from day 1 to day 10) showed both regional ischemia and hyperemia.³⁶ Although most of the human studies involved severe TBI, but subjects with minor head injuries also shown to have diminished response to blood pressure changes 48 h after injury.³⁸

Animal models permit more invasive and longitudinal imaging, but still, there are few reports describing effects of brain injury at time points >72 h. Early models of autoregulation of CBF after injury were performed in cats^{40,41} or rats⁴² in the acute period after

injury. In one report, discrete areas of uncoupling of CBF and metabolism after head injury were described in a rat model.⁴³ However, these findings were predominantly observed at the boundary zone within 1 mm of the contusion, at a time point 2 h after injury. Another rodent model used longitudinal imaging in a rat model to show that CBF was globally reduced at 30 min and 1 h after injury. At 2 h, only focal reduction of regional CBF in the cerebral tissue surrounding the trauma site was observed, resolved by 4 h after injury.⁴⁴ In another rodent study, TBI altered peri-lesional cerebral blood volume for over 4 days thereafter gradually recovering. Other studies in rodent models focused on the changes in regional and global CBF (not local hyperemia) and at time points ranging from 5 min to 72 h.^{10,45–54} We are not aware of any other studies in rodent models that have either reported changes in local CBF regulation at later time points or measured cerebrovascular responses to capillary K^+ stimulation.

Pressure injection of K^+ could affect other brain cell types to release vasoactive mediators contributing to hyperemic response. Our previous work rules out indirect effects of pressure ejection of K^+ through depolarization of neurons as a mechanism for hyperemic responses because blockade of neuronal action potentials with tetrodotoxin did not prevent these responses.⁷ Furthermore, barium could have a direct effect on neural activity, but we and others have shown that barium at concentrations of 100 μ M or more does not affect cortical neuronal activity *in vivo*.^{7,55} While our current results convincingly demonstrate altered capillary-to-arteriolar communication, we have not excluded other potential mechanisms that might contribute to impaired vasodilatory responses, such as cerebral edema,⁵⁶ upregulation of aquaporins or disruption of glymphatic networks,^{57,58} effects on pericytes,^{59–62} perivascular inflammation, astrogliosis, and tau protein pathology.³⁰ We also acknowledge that imaging in awake mice differs from those under anesthesia. Specifically, compared to awake mice, cardiovascular responses and neurovascular coupling are slightly blunted in mice when they are anesthetized, resulting in a decrease in CBF and increased oxygen partial pressure.^{63–66}

While it is theoretically possible that the anesthesia and surgical procedure, and not the fluid percussion injury, impacted the Kir response, we would contend that the significant mechanical neurotrauma is far more likely to be the culprit. We acknowledge that laser doppler scanning studies have shown that in mice, isoflurane increases regional blood flow in a dose-dependent manner, these effects occur while the animals are under anesthesia, and not subsequently.^{67,68} The pulmonary washout of isoflurane occurs within minutes, and metabolism is negligible,⁶⁹ and in mice,

levels are undetectable in the brain 24 h after treatment.⁷⁰ The half-life of buprenorphine in mice is only about 3 h, and by 12 h, the analgesic properties of buprenorphine have already dissipated.⁷¹ Cutaneous incisions in mice heal quickly when closed with sutures under tension, achieving tensile strength with 5–7 days.⁷² The healing scalp wound should not impact local regulation of CBF. Thus, taken together, it is unlikely that either the anesthesia or the surgical procedure would produce any confounding effects by the time at which we studied animals, 3–7 days after surgery. Our observations that K⁺-induced hyperemia is comparable in naïve and sham control mice (Supplementary Figure 1) further support our premise that the effects are due to neurotrauma and not the surgical procedure.

Although we did not specifically evaluate the role of Kir2.1 in the observed *in vivo* response after TBI, we previously confirmed that cEC Kir2.1 channels are critical to K⁺-mediated, capillary-based communication mechanisms as *in vivo* local hyperemic responses resulted selectively blocked by BaCl₂ (100 μM) or absent in EC Kir2.1^{-/-} mice.⁷ We would not expect further reduction in K⁺ responses after TBI by adding BaCl₂ or in a Kir2.1 ablation model. Therefore, patch clamp electrophysiology was employed to establish the role of Kir2.1 channel dysfunction in the disruption of capillary-to-arteriolar electrical signaling after TBI.

TBI resulted in a ~60% reduction in cEC Kir channel function

Given our recent insights into the critical role of cECs in electro-chemical signaling during functional hyperemia,⁷ we hypothesized that abnormal K⁺-induced hyperemic response after TBI is due to a reduction in cEC Kir2.1 channel function. Indeed, we saw a significant reduction in Kir2.1 channel density in freshly isolated cECs isolated from TBI mice. Although the role of cEC Kir channels has not previously been investigated in models of ischemia or brain injury, these findings align with our previous results showing an attenuation of penetrating arterioles smooth muscle Kir channel function after transient global ischemia that caused a reduction in K⁺-induced vasodilation of pial arteries.⁷³

Capillary EC Kir2.1 channels are dynamically regulated by membrane phospholipids such as phosphatidylinositol 4,5-bisphosphate (PIP₂)⁷⁴ and G_qPCR activity.⁷⁵ Trauma and shock result in pronounced alterations in lipid metabolism.^{76–78} Thus, reduced cEC Kir2.1 channel function may be attributed to changes in lipid metabolism resulting in reduced PIP₂ levels. Interestingly, gain-of-function of mutation

in the G_{α_q} protein, encoded by *GNAQ* in the patients with Sturge–Weber syndrome is associated with reduced cerebral perfusion suggesting possible association of reduced CBF after TBI with PIP₂.^{79,80} Because global alterations in vascular PIP₂ would be expected to impact Kir2.1 function not only in capillaries, but also in larger vessels, we next sought to establish the extent to which isolated cerebral arteries responded to K⁺ exposure.

Diminished K⁺-induced vasodilation extends to isolated cerebral arteries

We hypothesized that cerebral arteries isolated after TBI would also show functional impairment in vasodilatory responses to K⁺. Here, we show that TBI impairs the response to extracellular K⁺ (10 mM) in cerebral arteries despite a normal response to pressure-induced constriction (myogenic tone) at 80 mm Hg. To our knowledge, this is the first report of K⁺-induced dilation in isolated blood vessels after TBI.

Our finding of a preserved myogenic response to pressure (80 mm Hg) in cerebral arteries from TBI mice stands in contrast with other studies of myogenic tone in isolated vessels at earlier time points after TBI. For example, two prior reports demonstrated reduced middle cerebral artery dilation 2-h post-TBI,^{45,81} and a third report showed abnormal middle cerebral artery responses at 24 h but not 2 h or 120 h after injury.⁸² We have previously demonstrated that in a rat model of TBI, 24 h after injury, cerebral arteries develop a profound gain-of-function in nitric oxide generation, due to upregulation of inducible nitric oxide synthase, causing a loss of the myogenic response in both ipsilateral and contralateral pial arteries.⁸³ However, any nitric oxide elevation and accompanying reduction in myogenic tone present at 2–24 h may have resolved by the time points we used for our study, 4–7 days after injury.

Our results also suggest that endothelial Kir dysfunction after trauma is not limited to capillaries and extends to pial arteries. The diminished response to extracellular K⁺ observed in isolated cerebral arterial preparations likely involves both endothelial Kir channels as well as those expressed in vascular smooth muscle cells. Smooth muscle Kir channels play a major role in the regulation of vascular tone of cerebral arteries, and impaired penetrating arteriolar smooth muscle Kir channel function was previously reported in a model of global cerebral ischemia.^{73,84} Although not previously studied in TBI, altered cerebral artery responses to K⁺ in hemorrhagic stroke,^{85,86} stress,⁸⁷ hypoxia,⁸⁸ and in other vascular ion channels, such as large conductance Ca²⁺-activated K⁺ channels have previously been described.⁸⁹ Altered pial vessel responses to K⁺ after TBI would be expected to

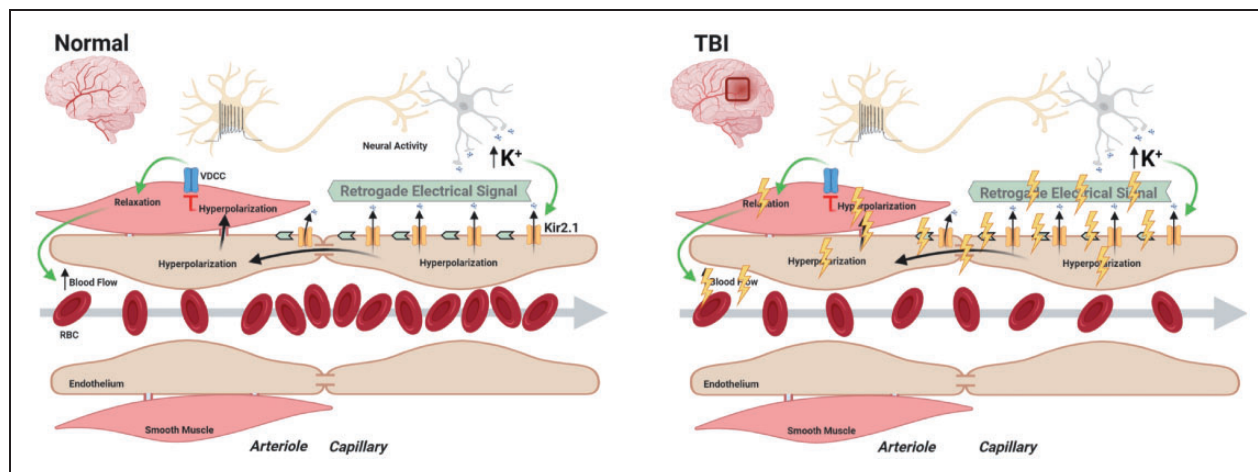


Figure 6. Proposed mechanism showing impairment of electrical signaling after TBI. Left panel represents healthy brain where neural activity driven increase in extracellular K^+ causes activation of capillary endothelial cell Kir2.1 channels to initiate propagating hyperpolarization (electrical signal) towards upstream penetrating arterioles, these hyperpolarizing signals inhibit voltage gated Ca^{2+} channels (VDCCs) to relax smooth muscle cells causing dilation of the penetrating arterioles to increase CBF. Right panel represents pathophysiology of TBI on the brain resulting in disruption of capillary-to-arteriolar electrical signaling and impaired K^+ -driven hyperemic response.

contribute to impaired K^+ -induced hyperemia and reduced local CBF, in addition to the disrupted capillary-to-arteriole signaling.

Conclusions

Collectively, our study addresses a critical knowledge gap in TBI that not only increases our mechanistic understanding of local CBF regulation after injury, but also, may lead to new strategies for treating long-term disabilities after TBI. We have shown for the first time that survivable TBI has long-term effects on cerebral capillary function and the dynamic regulation of local CBF responses during neurovascular coupling (Figure 6). Our demonstration of Kir2.1 dysfunction as a mechanism which underlies impaired capillary-to-arteriolar signaling after TBI provides a rationale for therapeutic approaches to rescue Kir2.1 channel function through membrane PIP_2 . Such manipulations might be expected to restore local CBF regulation and improve the quality of life for athletes, military servicemen and women, and other survivors of head injuries.

Funding

The author(s) disclosed receipt of the following financial support for the research, authorship, and/or publication of this article: This study was supported by the American Heart Association (20POST35210155 and 17SDG33670237), Department of Defense/The Henry M. Jackson Foundation for the Advancement of Military Medicine (HU001-18-2-0016), National Institutes of Health (RO1GM123010, R01NS110656, R35HL140027, and R37DK053832), EC

Horizon 2020, Fondation Leducq, and the Totman Medical Research Trust.

Data accessibility

All underlying research data supporting the findings of this study, such as electrical recordings, pressure myography tracings, and video images, can be accessed upon request.

Declaration of conflicting interests

The author(s) declared no potential conflicts of interest with respect to the research, authorship, and/or publication of this article.

Author contributions

AM designed experiments, acquired, and analyzed data, wrote the initial draft and edited all subsequent drafts of the manuscript. AMS acquired and analyzed myograph data and participated in all stages of critical revisions. MS acquired and analyzed electrophysiology data. SR performed surgeries to induce fluid percussion injury. TAL, WL, MTN, and KF conceived and designed the overall study and experimental series. MTN and KF directed the study and edited the manuscript. All authors reviewed the manuscript, contributed to critical revisions, and approved its submission.

Supplemental material

Supplemental material for this article is available online.

References

1. Dewan MC, Rattani A, Gupta S, et al. Estimating the global incidence of traumatic brain injury. *J Neurosurg* 2018; 1: 1–18.

2. Taylor CA, Bell JM, Breiding MJ, et al. Traumatic brain injury-related emergency department visits, hospitalizations, and deaths – United States, 2007 and 2013. *MMWR Surveill Summ* 2017; 66: 1–16.
3. Marin JR, Weaver MD, Yealy DM, et al. Trends in visits for traumatic brain injury to emergency departments in the United States. *JAMA* 2014; 311: 1917–1919.
4. Abdul-Muneer PM, Conte AA, Haldar D, et al. Traumatic brain injury induced matrix metalloproteinase-2 cleaves CXCL12alpha (stromal cell derived factor 1alpha) and causes neurodegeneration. *Brain Behav Immun* 2017; 59: 190–199.
5. Roozenbeek B, Maas AI and Menon DK. Changing patterns in the epidemiology of traumatic brain injury. *Nat Rev Neurol* 2013; 9: 231–236.
6. Wojcik BE, Stein CR, Bagg K, et al. Traumatic brain injury hospitalizations of U.S. army soldiers deployed to Afghanistan and Iraq. *Am J Prev Med* 2010; 38: S108–116.
7. Longden TA, Dabertrand F, Koide M, et al. Capillary K (+)-sensing initiates retrograde hyperpolarization to increase local cerebral blood flow. *Nat Neurosci* 2017; 20: 717–726.
8. Hlatky R, Goodman JC, Valadka AB, et al. Role of nitric oxide in cerebral blood flow abnormalities after traumatic brain injury. *J Cereb Blood Flow Metab* 2003; 23: 582–588.
9. Ostergaard L, Engedal TS, Aamand R, et al. Capillary transit time heterogeneity and flow-metabolism coupling after traumatic brain injury. *J Cereb Blood Flow Metab* 2014; 34: 1585–1598.
10. Golding EM, Robertson CS, Fitch JC, et al. Segmental vascular resistance after mild controlled cortical impact injury in the rat. *J Cereb Blood Flow Metab* 2003; 23: 210–218.
11. Salehi A, Zhang JH and Obenaus A. Response of the cerebral vasculature following traumatic brain injury. *J Cereb Blood Flow Metab* 2017; 37: 2320–2339.
12. Abrahamson EE and Ikonovic MD. Brain injury-induced dysfunction of the blood brain barrier as a risk for dementia. *Exp Neurol* 2020; 328: 113257.
13. Sigurdardottir S, Andelic N, Roe C, et al. Trajectory of 10-year neurocognitive functioning after moderate-severe traumatic brain injury: early associations and clinical application. *J Int Neuropsychol Soc* 2020; 26: 654–667.
14. Raj R, Kaprio J, Korja M, et al. Risk of hospitalization with neurodegenerative disease after moderate-to-severe traumatic brain injury in the working-age population: a retrospective cohort study using the Finnish national health registries. *PLoS Med* 2017; 14: e1002316.
15. Vadlamani A and Albrecht JS. Severity of traumatic brain injury in older adults and risk of ischemic stroke and depression. *J Head Trauma Rehabil* 2020; 35: E436–E440.
16. Enevoldsen EM, Cold G, Jensen FT, et al. Dynamic changes in regional CBF, intraventricular pressure, CSF pH and lactate levels during the acute phase of head injury. *J Neurosurg* 1976; 44: 191–214.
17. Langfitt TW, Obrist WD, Gennarelli TA, et al. Correlation of cerebral blood flow with outcome in head injured patients. *Ann Surg* 1977; 186: 411–414.
18. Enevoldsen EM and Jensen FT. Autoregulation and CO₂ responses of cerebral blood flow in patients with acute severe head injury. *J Neurosurg* 1978; 48: 689–703.
19. Sackheim AM, Stockwell D, Villalba N, et al. Traumatic brain injury impairs sensorimotor function in mice. *J Surg Res* 2017; 213: 100–109.
20. Yardeni T, Eckhaus M, Morris HD, et al. Retro-orbital injections in mice. *Lab Anim (NY)* 2011; 40: 155–160.
21. Montoya-Zegarra JA, Russo E, Runge P, et al. AutoTube: a novel software for the automated morphometric analysis of vascular networks in tissues. *Angiogenesis* 2019; 22: 223–236.
22. Dawes GS. The vaso-dilator action of potassium. *J Physiol (Lond)* 1941; 99: 224–238.
23. Nakahata K, Kinoshita H, Tokinaga Y, et al. Vasodilation mediated by inward rectifier K⁺ channels in cerebral microvessels of hypertensive and normotensive rats. *Anesth Analg* 2006; 102: 571–576.
24. Nelson MT and Quayle JM. Physiological roles and properties of potassium channels in arterial smooth muscle. *Am J Physiol* 1995; 268: C799–822.
25. McCarron JG and Halpern W. Potassium dilates rat cerebral arteries by two independent mechanisms. *Am J Physiol* 1990; 259: H902–908.
26. Haber M, Amyot F, Kenney K, et al. Vascular abnormalities within normal appearing tissue in chronic traumatic brain injury. *J Neurotrauma* 2018; 35: 2250–2258.
27. Obenaus A, Ng M, Orantes AM, et al. Traumatic brain injury results in acute rarefaction of the vascular network. *Sci Rep* 2017; 7: 239.
28. Rodriguez-Baeza A, Reina-de la Torre F, Poca A, et al. Morphological features in human cortical brain microvessels after head injury: a three-dimensional and immunocytochemical study. *Anat Rec A Discov Mol Cell Evol Biol* 2003; 273: 583–593.
29. Stein SC, Graham DI, Chen XH, et al. Association between intravascular microthrombosis and cerebral ischemia in traumatic brain injury. *Neurosurgery* 2004; 54: 687–691; discussion 691.
30. Tagge CA, Fisher AM, Minaeva OV, et al. Concussion, microvascular injury, and early tauopathy in young athletes after impact head injury and an impact concussion mouse model. *Brain* 2018; 141: 422–458.
31. Longden TA, Hill-Eubanks DC and Nelson MT. Ion channel networks in the control of cerebral blood flow. *J Cereb Blood Flow Metab* 2016; 36: 492–512.
32. Blinder P, Shih AY, Rafie C, et al. Topological basis for the robust distribution of blood to rodent neocortex. *Proc Natl Acad Sci USA* 2010; 107: 12670–12675.
33. Shih AY, Blinder P, Tsai PS, et al. The smallest stroke: occlusion of one penetrating vessel leads to infarction and a cognitive deficit. *Nat Neurosci* 2013; 16: 55–63.
34. Robertson CS, Contant CF, Gokaslan ZL, et al. Cerebral blood flow, arteriovenous oxygen difference, and outcome in head injured patients. *J Neurol Neurosurg Psychiatry* 1992; 55: 594–603.

35. Wei HS, Kang H, Rasheed ID, et al. Erythrocytes are oxygen-sensing regulators of the cerebral microcirculation. *Neuron* 2016; 91: 851–862.
36. Launey Y, Fryer TD, Hong YT, et al. Spatial and temporal pattern of ischemia and abnormal vascular function following traumatic brain injury. *JAMA Neurol* 2020; 77: 339–349.
37. Xu Y, McArthur DL, Alger JR, et al. Early nonischemic oxidative metabolic dysfunction leads to chronic brain atrophy in traumatic brain injury. *J Cereb Blood Flow Metab* 2010; 30: 883–894.
38. Junger EC, Newell DW, Grant GA, et al. Cerebral autoregulation following minor head injury. *J Neurosurg* 1997; 86: 425–432.
39. Overgaard J and Tweed WA. Cerebral circulation after head injury. 1. Cerebral blood flow and its regulation after closed head injury with emphasis on clinical correlations. *J Neurosurg* 1974; 41: 531–541.
40. Lewelt W, Jenkins LW and Miller JD. Autoregulation of cerebral blood flow after experimental fluid percussion injury of the brain. *J Neurosurg* 1980; 53: 500–511.
41. DeWitt DS, Jenkins LW, Wei EP, et al. Effects of fluid-percussion brain injury on regional cerebral blood flow and pial arteriolar diameter. *J Neurosurg* 1986; 64: 787–794.
42. Ekelund L, Nilsson B and Ponten U. Carotid angiography after experimental head injury in the rat. *Neuroradiology* 1974; 7: 209–214.
43. Richards HK, Simac S, Piechnik S, et al. Uncoupling of cerebral blood flow and metabolism after cerebral contusion in the rat. *J Cereb Blood Flow Metab* 2001; 21: 779–781.
44. Yamakami I and McIntosh TK. Alterations in regional cerebral blood flow following brain injury in the rat. *J Cereb Blood Flow Metab* 1991; 11: 655–660.
45. Rodriguez UA, Zeng Y, Deyo D, et al. Effects of mild blast traumatic brain injury on cerebral vascular, histopathological, and behavioral outcomes in rats. *J Neurotrauma* 2018; 35: 375–392.
46. Buckley EM, Miller BF, Golinski JM, et al. Decreased microvascular cerebral blood flow assessed by diffuse correlation spectroscopy after repetitive concussions in mice. *J Cereb Blood Flow Metab* 2015; 35: 1995–2000.
47. Bir C, Vandevord P, Shen Y, et al. Effects of variable blast pressures on blood flow and oxygen saturation in rat brain as evidenced using MRI. *Magn Reson Imaging* 2012; 30: 527–534.
48. Thomale UW, Kroppenstedt SN, Beyer TF, et al. Temporal profile of cortical perfusion and microcirculation after controlled cortical impact injury in rats. *J Neurotrauma* 2002; 19: 403–413.
49. Engelborghs K, Haseldonckx M, Van Reempts J, et al. Impaired autoregulation of cerebral blood flow in an experimental model of traumatic brain injury. *J Neurotrauma* 2000; 17: 667–677.
50. DeWitt DS, Smith TG, Deyo DJ, et al. L-arginine and superoxide dismutase prevent or reverse cerebral hypoperfusion after fluid-percussion traumatic brain injury. *J Neurotrauma* 1997; 14: 223–233.
51. Nilsson P, Gazelius B, Carlson H, et al. Continuous measurement of changes in regional cerebral blood flow following cortical compression contusion trauma in the rat. *J Neurotrauma* 1996; 13: 201–207.
52. Bryan RM Jr., Cherian L and Robertson C. Regional cerebral blood flow after controlled cortical impact injury in rats. *Anesth Analg* 1995; 80: 687–695.
53. Yuan XQ, Prough DS, Smith TL, et al. The effects of traumatic brain injury on regional cerebral blood flow in rats. *J Neurotrauma* 1988; 5: 289–301.
54. Muir JK, Boerschel M and Ellis EF. Continuous monitoring of posttraumatic cerebral blood flow using laser-Doppler flowmetry. *J Neurotrauma* 1992; 9: 355–362.
55. Leithner C, Roysl G, Offenhauser N, et al. Pharmacological uncoupling of activation induced increases in CBF and CMRO₂. *J Cereb Blood Flow Metab* 2010; 30: 311–322.
56. Immonen R, Heikkinen T, Tahtivaara L, et al. Cerebral blood volume alterations in the perilesional areas in the rat brain after traumatic brain injury—comparison with behavioral outcome. *J Cereb Blood Flow Metab* 2010; 30: 1318–1328.
57. Iliff JJ, Chen MJ, Plog BA, et al. Impairment of glymphatic pathway function promotes tau pathology after traumatic brain injury. *J Neurosci* 2014; 34: 16180–16193.
58. Ren Z, Iliff JJ, Yang L, et al. Hit & run’ model of closed-skull traumatic brain injury (TBI) reveals complex patterns of post-traumatic AQP4 dysregulation. *J Cereb Blood Flow Metab* 2013; 33: 834–845.
59. Hill RA, Tong L, Yuan P, et al. Regional blood flow in the normal and ischemic brain is controlled by arteriolar smooth muscle cell contractility and not by capillary pericytes. *Neuron* 2015; 87: 95–110.
60. Fernandez-Klett F and Priller J. Diverse functions of pericytes in cerebral blood flow regulation and ischemia. *J Cereb Blood Flow Metab* 2015; 35: 883–887.
61. Hall CN, Reynell C, Gesslein B, et al. Capillary pericytes regulate cerebral blood flow in health and disease. *Nature* 2014; 508: 55–60.
62. Peppiatt CM, Howarth C, Mobbs P, et al. Bidirectional control of CNS capillary diameter by pericytes. *Nature* 2006; 443: 700–704.
63. Gao YR, Ma Y, Zhang Q, et al. Time to wake up: studying neurovascular coupling and brain-wide circuit function in the un-anesthetized animal. *Neuroimage* 2017; 153: 382–398.
64. Masamoto K and Kanno I. Anesthesia and the quantitative evaluation of neurovascular coupling. *J Cereb Blood Flow Metab* 2012; 32: 1233–1247.
65. Aksenov DP, Li L, Miller MJ, et al. Effects of anesthesia on BOLD signal and neuronal activity in the somatosensory cortex. *J Cereb Blood Flow Metab* 2015; 35: 1819–1826.
66. Lyons DG, Parpaleix A, Roche M, et al. Mapping oxygen concentration in the awake mouse brain. *Elife* Epub ahead of print 03 February 2016. DOI: 10.7554/eLife.12024.

67. Okamoto H, Meng W, Ma J, et al. Isoflurane-induced cerebral hyperemia in neuronal nitric oxide synthase gene deficient mice. *Anesthesiology* 1997; 86: 875–884.
68. Kehl F, Shen H, Moreno C, et al. Isoflurane-induced cerebral hyperemia is partially mediated by nitric oxide and epoxyeicosatrienoic acids in mice in vivo. *Anesthesiology* 2002; 97: 1528–1533.
69. Holaday DA, Fiserova-Bergerova V, Latta IP, et al. Resistance of isoflurane to biotransformation in man. *Anesthesiology* 1975; 43: 325–332.
70. Sonner JM, Werner DF, Elsen FP, et al. Effect of isoflurane and other potent inhaled anesthetics on minimum alveolar concentration, learning, and the righting reflex in mice engineered to express alpha gamma-aminobutyric acid type A receptors unresponsive to isoflurane. *Anesthesiology* 2007; 106: 107–113.
71. Gargiulo S, Greco A, Gramanzini M, et al. Mice anesthesia, analgesia, and care, part I: anesthetic considerations in preclinical research. *Illar J* 2012; 53: E55–69.
72. Pickett BP, Burgess LP, Livermore GH, et al. Wound healing. Tensile strength vs healing time for wounds closed under tension. *Arch Otolaryngol Head Neck Surg* 1996; 122: 565–568.
73. Povlsen GK, Longden TA, Bonev AD, et al. Uncoupling of neurovascular communication after transient global cerebral ischemia is caused by impaired parenchymal smooth muscle Kir channel function. *J Cereb Blood Flow Metab* 2016; 36: 1195–1201.
74. Harraz OF, Longden TA, Dabertrand F, et al. Endothelial GqPCR activity controls capillary electrical signaling and brain blood flow through PIP2 depletion. *Proc Natl Acad Sci USA* 2018; 115: E3569–E3577.
75. Harraz OF, Longden TA, Hill-Eubanks D, et al. PIP2 depletion promotes TRPV4 channel activity in mouse brain capillary endothelial cells. *Elife* 2018; 7: e38689.
76. Abdullah L, Evans JE, Ferguson S, et al. Lipidomic analyses identify injury-specific phospholipid changes 3 mo after traumatic brain injury. *Faseb J* 2014; 28: 5311–5321.
77. Emmerich T, Abdullah L, Crynen G, et al. Plasma lipidomic profiling in a military population of mild traumatic brain injury and post-traumatic stress disorder with apolipoprotein E varepsilon4-dependent effect. *J Neurotrauma* 2016; 33: 1331–1348.
78. Hogan SR, Phan JH, Alvarado-Velez M, et al. Discovery of lipidome alterations following traumatic brain injury via high-resolution metabolomics. *J Proteome Res* 2018; 17: 2131–2143.
79. Shirley MD, Tang H, Gallione CJ, et al. Sturge-Weber syndrome and port-wine stains caused by somatic mutation in GNAQ. *N Engl J Med* 2013; 368: 1971–1979.
80. Huang L, Couto JA, Pinto A, et al. Somatic GNAQ mutation is enriched in brain endothelial cells in Sturge-Weber syndrome. *Pediatr Neurol* 2017; 67: 59–63.
81. Mathew BP, DeWitt DS, Bryan RM Jr, et al. Traumatic brain injury reduces myogenic responses in pressurized rodent middle cerebral arteries. *J Neurotrauma* 1999; 16: 1177–1186.
82. Golding EM, Contant CF Jr., Robertson CS, et al. Temporal effect of severe controlled cortical impact injury in the rat on the myogenic response of the middle cerebral artery. *J Neurotrauma* 1998; 15: 973–984.
83. Villalba N, Sonkusare SK, Longden TA, et al. Traumatic brain injury disrupts cerebrovascular tone through endothelial inducible nitric oxide synthase expression and nitric oxide gain of function. *J Am Heart Assoc* 2014; 3: 12–21.
84. Zaritsky JJ, Eckman DM, Wellman GC, et al. Targeted disruption of Kir2.1 and Kir2.2 genes reveals the essential role of the inwardly rectifying K(+) current in K(+) mediated vasodilation. *Circ Res* 2000; 87: 160–166.
85. Balbi M, Koide M, Wellman GC, et al. Inversion of neurovascular coupling after subarachnoid hemorrhage in vivo. *J Cereb Blood Flow Metab* 2017; 37: 3625–3634.
86. Pappas AC, Koide M and Wellman GC. Astrocyte Ca2+ signaling drives inversion of neurovascular coupling after subarachnoid hemorrhage. *J Neurosci* 2015; 35: 13375–13384.
87. Longden TA, Dabertrand F, Hill-Eubanks DC, et al. Stress-induced glucocorticoid signaling remodels neurovascular coupling through impairment of cerebrovascular inwardly rectifying K+ channel function. *Proc Natl Acad Sci USA* 2014; 111: 7462–7467.
88. Somjen GG. Mechanisms of spreading depression and hypoxic spreading depression-like depolarization. *Physiol Rev* 2001; 81: 1065–1096.
89. Toth P, Szarka N, Farkas E, et al. Traumatic brain injury-induced autoregulatory dysfunction and spreading depression-related neurovascular uncoupling: pathomechanisms, perspectives, and therapeutic implications. *Am J Physiol Heart Circ Physiol* 2016; 311: H1118–H1131.